https://doi.org/10.1038/s41586-019-1061-2

Nonreciprocal control and cooling of phonon modes in an optomechanical system

H. Xu[1,2], Luyao Jiang[1], A. A. Clerk[3] & J. G. E. Harris[1,4]*

Mechanical resonators are important components of devices that range from gravitational wave detectors to cellular telephones. They serve as high-performance transducers, sensors and filters by offering low dissipation, tunable coupling to diverse physical systems, and compatibility with a wide range of frequencies, materials and fabrication processes. Systems of mechanical resonators typically obey reciprocity, which ensures that the phonon transmission coefficient between any two resonators is independent of the direction of transmission[1,2]. Reciprocity must be broken to realize devices (such as isolators and circulators) that provide one-way propagation of acoustic energy between resonators. Such devices are crucial for protecting active elements, mitigating noise and operating full-duplex transceivers. Until now, nonreciprocal phononic devices[3–11] have not simultaneously combined the features necessary for robust operation: strong nonreciprocity, in situ tunability, compact integration and continuous operation. Furthermore, they have been applied only to coherent signals (rather than fluctuations or noise), and have been realized exclusively in travelling-wave systems (rather than resonators). Here we describe a scheme that uses the standard cavity-optomechanical interaction to produce robust nonreciprocal coupling between phononic resonators. This scheme provides about 30 decibels of isolation in continuous operation and can be tuned in situ simply via the phases of the drive tones applied to the cavity. In addition, by directly monitoring the dynamics of the resonators we show that this nonreciprocity can control thermal fluctuations, and that this control represents a way to cool phononic resonators.

Reciprocity is a generic feature of linear, time-invariant oscillator systems. It may be broken in various ways, such as by introducing bias, nonlinearity or parametric time dependence[1,2]. In phononic systems, nonreciprocal bias can be introduced by imposing rotational motion[9] or a magnetic field[3–5]. However, the former is impractical in many settings, and the latter typically produces weak nonreciprocity. Likewise, nonlinearity-based approaches[6–8] have required bulky components and generally result in signal distortion. By contrast, parametric modulation can produce nonreciprocity with considerable flexibility (as demonstrated recently for electromagnetic waves[12–18]).

Parametric modulation of phononic resonators arises naturally in cavity optomechanical systems, which consist of an electromagnetic cavity that is detuned by the motion of mechanical oscillators[19]. In particular, electromagnetic drive tones applied to the cavity can tune the mechanical oscillators' frequencies, dampings and couplings, an effect known as 'dynamical backaction'[19]. This effect has been used to realize transient nonreciprocity (by adding a slow time dependence to the parametric modulation[10,11]); by contrast, the scheme described here uses stationary modulation and operates continuously.

The phononic resonators studied here are two normal modes of a SiN membrane[20] with dimensions 1 mm × 1 mm × 50 nm. We focus on a pair of low-order drumhead-like modes with resonant frequencies $\omega_1 = 2\pi \times 557.473$ kHz and $\omega_2 = 2\pi \times 705.164$ kHz and damping rates $\gamma_1 = 2\pi \times 0.39$ Hz and $\gamma_2 = 2\pi \times 0.38$ Hz. The membrane is positioned inside a cryogenic Fabry–Perot optical cavity with linewidth $\kappa = 2\pi \times 180$ kHz and coupling rate $\kappa_{\mathrm{in}} = 2\pi \times 70$ kHz (for light with wavelength $\lambda = 1{,}064$ nm). The mechanical resonators couple to the cavity with rates $g_1 = 2\pi \times 2.11$ Hz and $g_2 = 2\pi \times 2.12$ Hz. The device construction and characterization are described in refs [10,11]. The wide separation between ω_1 and ω_2 enables the motion of both modes to be inferred from a single record of the cavity detuning, which is provided by a probe laser that drives the cavity with fixed intensity and detuning.

Near-resonant coupling can be induced between these modes by modulating the dynamical backaction at a frequency close to $\delta\omega \equiv \omega_1 - \omega_2$. Such modulation arises from the intracavity beat note produced when the cavity is driven by two tones, the detunings of which (relative to the cavity resonance) are[11,21,22]: $\Delta_1 = -\omega_1 + \Delta_\ell$ and $\Delta_2 = -\omega_2 + \Delta_\ell$. In this arrangement, a photon can scatter from one drive tone to the other by transferring a phonon between the modes. This process (illustrated by the red arrows in Fig. 1a, b) occurs via a virtual state in which the photon is at a mechanical sideband of the drive tones. The participation of the various mechanical sidebands can be enhanced or suppressed by the cavity's resonance; for the detunings shown in Fig. 1a, the cavity ensures that the sideband with detuning Δ_ℓ is the dominant path by which phonon transfer takes place.

This phonon transfer process has two crucial features. First, the transfer amplitude is proportional to the complex-valued cavity susceptibility $\chi(\Delta_\ell)$ (where $\chi(\omega) = (\kappa/2 - i\omega)^{-1}$) regardless of the direction of transfer, and so has both a dissipative and a coherent character. Second, the phase of the intracavity beat note appears explicitly in the transfer coefficient. While these features alone do not result in nonreciprocal energy transfer (for example, the beat note phase can be gauged away), interference between two such processes can break reciprocity[12,23–27]. To accomplish this, the experiments described here incorporate a second pair of drive tones (orange arrows in Fig. 1a). The detunings of the four tones Δ_1, Δ_2, Δ_3 and Δ_4 are chosen to provide two beat notes that each induce near-resonant coupling between the modes (that is, $\Delta_1 - \Delta_2 = \Delta_3 - \Delta_4 \approx \delta\omega$) and hence two distinct copies of the phonon transfer process. The four detunings Δ_1, Δ_2, Δ_3 and Δ_4 are also chosen so that the dominant mechanical sideband in each transfer process has a distinct detuning: $\Delta_\ell = \Delta_2 + \omega_2 \approx \Delta_1 + \omega_1$ and $\Delta_{\mathrm{u}} = \Delta_4 + \omega_2 \approx \Delta_3 + \omega_1$. As described below, interference between these two processes results in nonreciprocal energy transfer between the phonon modes. Moreover, this interference is controlled by the relative phase between the two beat notes (which cannot be gauged away).

This system can be described via the standard linearized optomechanical equations of motion for one cavity mode and two mechanical modes[19] (see Methods). The cavity mode is subject to a drive of the form $\sum_{n=1}^{4}\sqrt{P_n}\,\mathrm{e}^{i(\Delta_n t+\phi_n)}$ where P_n is the power of the nth tone. The detuning, power and phase (ϕ_n) of each tone is set by a microwave generator that produces the four tones from a single laser via an acousto-optic modulator. Adiabatically eliminating the cavity field leaves equations of motion for the two mechanical mode amplitudes

[1]Department of Physics, Yale University, New Haven, CT, USA. [2]School of Physics, Peking University, Beijing, China. [3]Institute for Molecular Engineering, University of Chicago, Chicago, IL, USA. [4]Department of Applied Physics, Yale University, New Haven, CT, USA. *e-mail: jack.harris@yale.edu

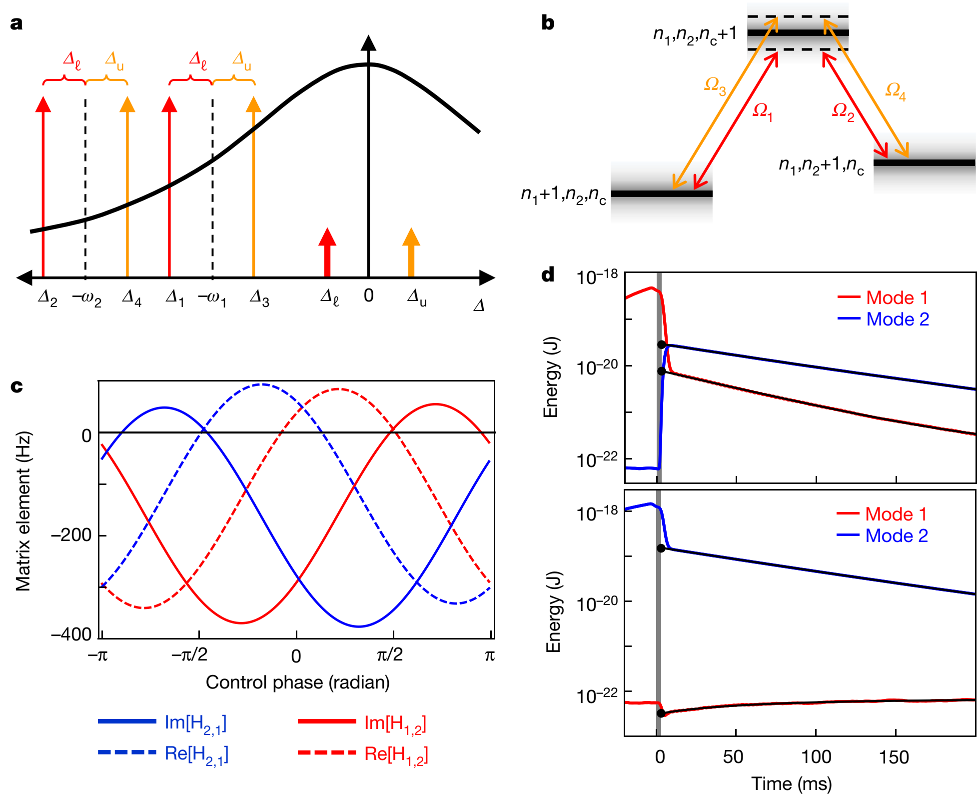

Fig. 1 | Optically induced mechanical nonreciprocity. a, Frequency-domain illustration of the optomechanical control scheme. The black curve is the cavity lineshape. The thin coloured arrows are control tones with detunings (relative to the cavity resonance) Δ_1, Δ_2, Δ_3 and Δ_4. Dashed lines are negative detunings equal to the frequencies of the phonon modes (ω_1,ω_2). The thick coloured arrows are motional sidebands that dominate the phonon transfer process (and which occur at detunings Δ_ℓ and Δ_u). The horizontal axis shows detuning from cavity resonance. **b**, The energy-domain illustration of the same scheme. The solid horizontal lines are states labelled by the number of phonons in each mode (n_1,n_2) and the number of cavity photons (n_c). The dashed horizontal lines are virtual states through which the transfer process occurs. The cavity linewidth is indicated by the grey shading. The absolute frequency of the ith control tone is Ω_i. **c**, The off-diagonal matrix elements of the effective Hamiltonian H as a function of the phase ϕ. The control beam powers and detunings are given in the main text. **d**, Measurement of the mechanical energy in each mode as a function of time. In the upper (lower) panel, mode 1 (2) is initially excited. The control beams are on only during the grey region (0 ms $\le t \le$ 3 ms). Data for $t >$ 3 ms is fitted to a decaying exponential (black curves) and this fit is extrapolated to t = 3 ms to find $\varepsilon_1(\tau)$ and $\varepsilon_2(\tau)$, the energies in each mode at the end of the control pulse (black dots). Identical control beams (with $\phi = \pi/2$) are used in both panels, but energy is transferred only from mode 1 to mode 2.

that correspond to the effective time-dependent Hamiltonian (see Methods):

$$H=\begin{pmatrix}\omega_1 - i\gamma_1/2 + f_1 & [g e^{i(\theta_\ell+\phi_{12})} + h e^{i(\theta_u+\phi_{34})}]e^{i\Delta t}\\ [g^* e^{i(\theta_\ell-\phi_{12})} + h^* e^{i(\theta_u-\phi_{34})}]e^{-i\Delta t} & \omega_2 - i\gamma_2/2 + f_2\end{pmatrix}$$

where t is time, $\Delta \equiv \Delta_1 - \Delta_2$ and $\theta_{\ell,u} \equiv \arg(-i(\chi(\Delta_{\ell,u}))$. The diagonal elements of H represent the usual single-tone dynamical backaction: $f_a \approx -i\sum_{n=1}^{4} P_n g_a^2 \hbar^{-1} |\chi(\Delta_n)|^2 \chi(\Delta_n + \omega_a)$ where $a \in \{1, 2\}$. By contrast, the off-diagonal components of H describe the coupling between the two mechanical modes mediated by the intracavity beat notes. The phases of these beat notes are $\phi_{12} \equiv \phi_1 - \phi_2$ and $\phi_{34} \equiv \phi_3 - \phi_4$. The coefficients are $g \approx -i\sqrt{P_1P_2}\, g_1 g_2 \hbar^{-1} \chi^*(\Delta_1)\chi(\Delta_2)|\chi(\Delta_\ell)|$ and $h \approx -i\sqrt{P_3P_4}\, g_1 g_2 \hbar^{-1} \chi^*(\Delta_3)\chi(\Delta_4)|\chi(\Delta_u)|$. For clarity, the present discussion ignores smaller terms in f, g and h that are due to non-resonant mechanical sidebands (these terms are included in the analysis and fits presented below, and in the full description in Methods).

Isolation between the two mechanical modes (corresponding to $|H_{1,2}| \ll |H_{2,1}|$ or $|H_{2,1}| \ll |H_{1,2}|$) can be achieved by first choosing P_n and Δ_n so that $|g|$ and $|h|$ are nearly equal. For the present device, this is realized with all the $P_n = 5\ \mu$W and $\Delta_n = \{-\omega_1 + \Delta_\ell + \zeta, -\omega_2 + \Delta_\ell, -\omega_1 + \Delta_u + \zeta, -\omega_2 + \Delta_u\}$ where $\Delta_\ell = -2\pi \times 60$ kHz and $\Delta_u = 2\pi \times 150$ kHz. The constant ζ is the detuning of the beat notes relative to $\delta\omega$, and is set to $2\pi \times 100$ Hz. With the condition $|g| \approx |h|$ satisfied, ϕ_{12} and ϕ_{34} may be adjusted via the microwave generator to ensure that one off-diagonal element of H nearly vanishes while the other does not. This is shown in Fig. 1c, which plots $H_{1,2}$ and $H_{2,1}$ as a function of $\phi \equiv \phi_{12} - \phi_{34}$. For $\phi \approx \pi/2$, H allows energy to flow from mode 1 to mode 2 but not vice versa. The situation is reversed when $\phi \approx -\pi/2$. By contrast, $\phi \approx 0$ gives $H_{1,2} \approx H_{2,1}$. This tunability between isolation, reciprocity and reversed isolation occurs while keeping the P_n and Δ_n fixed, and varying only the ϕ_n. This avoids cross-talk between the nonreciprocity and other device parameters (such as the mechanical frequencies, which depend only weakly on ϕ_n).

To demonstrate the tunability of the nonreciprocity, we measured the transfer of energy between the two modes for various choices of ϕ. Two measurements with $\phi = \pi/2$ are shown in Fig. 1d, which plots $\varepsilon_1(t)$ and $\varepsilon_2(t)$: the energy in each mode (as inferred from the probe beam). For $t < 0$ the control tones are off, and one mode is driven to an average energy of about 10^{-18} J (corresponding to an amplitude of about 5×10^{-11} m). The other mode is undriven, except by thermal fluctuations consistent with the bath temperature $T_{\mathrm{bath}} = 4.2$ K. At $t = 0$ the drive is turned off and the control tones are turned on for a duration $\tau = 3$ ms. For $t > \tau$ the control tones are off again. Figure 1d demonstrates the isolation described above: under the influence of control tones with $\phi = \pi/2$, an excitation prepared in mode 1 is transferred to mode 2 (upper panel) while an excitation prepared in mode 2 is not transferred to mode 1 (lower panel).

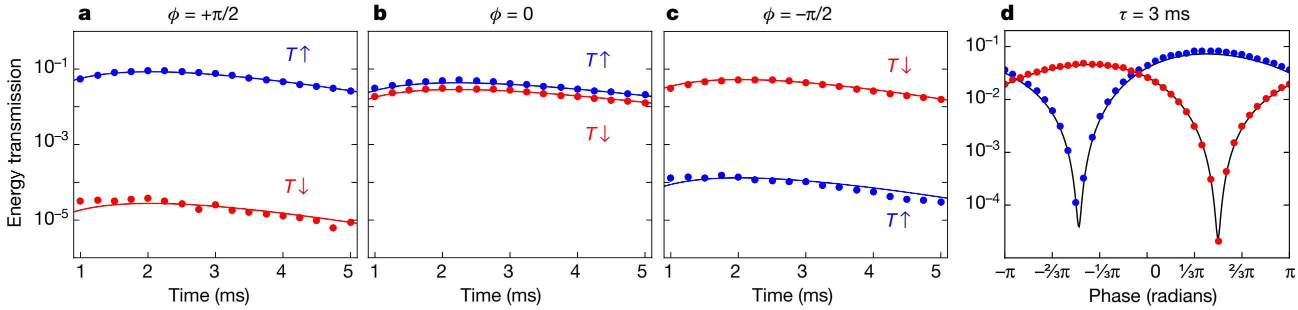

Fig. 2 | Nonreciprocal phonon transmission. The energy transmission coefficients $T_\uparrow$ and $T_\downarrow$ as a function of the control tones' duration τ (**a** to **c**) and phase ϕ (**d**). Each point is determined from measurements similar to those in Fig. 1d. The error bars for the statistical uncertainties are smaller than the symbols. The solid lines are the theoretical prediction described in the main text.

Figure 2 shows the energy transmission coefficients $T_\uparrow \equiv \varepsilon_2(\tau)/\varepsilon_1(0)$ and $T_\downarrow \equiv \varepsilon_1(\tau)/\varepsilon_2(0)$ (corresponding to transfer from mode 1 to mode 2 and vice versa) as a function of τ and ϕ. Both $T_\uparrow$ and $T_\downarrow$ decrease with τ, owing primarily to the damping induced by the single-tone backaction (all four control tones are red-detuned from the cavity resonance). However, the isolation ratio $I \equiv T_\uparrow/T_\downarrow$ is nearly independent of τ, as shown in Fig. 3a. We emphasize that while the measurements in Figs. 1–3 are carried out on excitations that are transient (owing to the modes' damping), the nonreciprocity is stationary. This is demonstrated explicitly in Fig. 3a and Fig. 4 (discussed below).

Figures 2d, 3b both show that reciprocity is restored (corresponding to $|H_{1,2}| = |H_{2,1}|$) for a value of ϕ that is very close to, but not exactly, zero, reflecting the fact that the nonreciprocity of H is determined by the phases θ_ℓ and θ_u as well as by ϕ. The data in Fig. 3 show that this system achieves $I \geq 30$ dB from mode 1 to mode 2 and $I \leq -25$ dB in the opposite direction. It also shows that I can be tuned over this entire range (including through 0 dB) by varying ϕ_n while all other parameters are held fixed. The solid lines in Figs. 2, 3 are not fits, but rather the time evolution predicted by the matrix exponential of H.

Experiments on nonreciprocal devices (in the phononic as well as other domains) typically measure the scattering matrix that describes propagating waves incident on and emanating from the device. By contrast, the measurements described here directly probe the device's internal degrees of freedom. This opens up the possibility of controlling the state of the resonators via their nonreciprocal interactions. To demonstrate this, we use the nonreciprocity described above to modify the thermal fluctuations of the resonators and to realize a form of cooling with no equivalent in reciprocal systems.

To describe the system's steady-state fluctuations, we note that both modes couple to the thermal bath ($T_{\mathrm{bath}} = 4.2$ K) and to the cavity field (the effective temperature of which can be approximated as zero for the present discussion[19,28]). In the absence of coupling between the phonon modes, these two 'baths' would cause each mode to equilibrate to a temperature $T_a = (\gamma_a/2\mathrm{Im}[f_a])T_{\mathrm{bath}}$ where $a \in \{1, 2\}$ and we assume the single-tone optical damping $\mathrm{Im}[f_a] \gg \gamma_a$. This reduction of T_a with respect to T_{bath} is the well-known effect of 'cold damping' or 'laser cooling'.[19] However, in the present system the modes also couple to each other. When the resulting energy transport is reciprocal ($|H_{1,2}| = |H_{2,1}|$) thermal phonons are exchanged between the modes, tending to bring T_1 and T_2 closer together. By contrast, if H is chosen to give unidirectional energy transport (for example, for $\phi = \pm\pi/2$), then the isolated mode emits thermal phonons into the other mode but not vice versa. This leads to cooling of the isolated mode and heating of the other mode, even if the former is initially the colder of the two.

To realize this isolation-based cooling we use the same Δ_n as above and $P_n = 2.5$ μW (resulting in $H_{1,2}$ and $H_{2,1}$ as in Fig. 1c but reduced by a factor of two). No external drive is applied to the phonon modes, and their undriven motion is recorded by the probe laser. Figure 4a shows the spectral density of each oscillator's energy S_{E_1} and S_{E_2} for $\phi = -\pi/2$, 0 and $+\pi/2$. For all values of ϕ, the mechanical linewidth is dominated by $\mathrm{Im}[f_a]$ (which is independent of ϕ). Asymmetric lineshapes are commonly observed in coupled damped oscillators with nearly degenerate modes;[29,30] however, in the present system the modes are non-degenerate and the lineshapes reflect interference between the two paths by which the thermal bath drives a given mode. For example, mode 1 is driven directly by bath fluctuations at frequencies near 557 kHz, but also by bath fluctuations near 705 kHz, which are first filtered by the response of mode 2 and then transferred to frequencies near 557 kHz by H. The solid lines in Fig. 4a are fits to the expected form (a constant background plus the square modulus of the sum of two Lorentzians).

To measure the effect of nonreciprocity on the mode temperatures, T_1 and T_2 are determined from the area under the peaks in S_{E_1} and S_{E_2} at several values of ϕ (see Methods and Extended Data Fig. 1). The result is plotted in Fig. 4b as the normalized temperature difference $\Theta(\phi) \equiv 1 - (T_2(\phi)/T_1(\phi)) / \langle T_2/T_1 \rangle$ where $\langle \ldots \rangle$ denotes the average over ϕ. Maximizing the isolation between the modes (that is, setting $\phi = \pm\pi/2$) results in the most extreme values of Θ. We emphasize that changing the sign of Θ is equivalent to reversing the direction of heat flow between the modes. As $\langle T_2/T_1 \rangle = 1.79 > 1$ in these measurements, heat is transported from the colder mode to the hotter mode when $\Theta < 0$.

The solid line in Fig. 4b shows Θ as calculated from the optomechanical equations of motion (Methods). The agreement between the measured and predicted cooling extends over a wide range of parameters, as illustrated in Fig. 4b–e, which shows $\Theta(\phi)$ for various Δ_n. The main effect of varying Δ_n is to increase the difference between $|g|$ and $|h|$, which results in weakened isolation and suppression of Θ.

We also emphasize that the data in each panel of Fig. 4b–e were taken with fixed P_n and Δ_n, and that the additional cooling of one mode is accomplished just by varying the phases of the control tones. Because conventional laser cooling techniques (for example, those using the single-tone dynamical backaction) are independent of these phases,

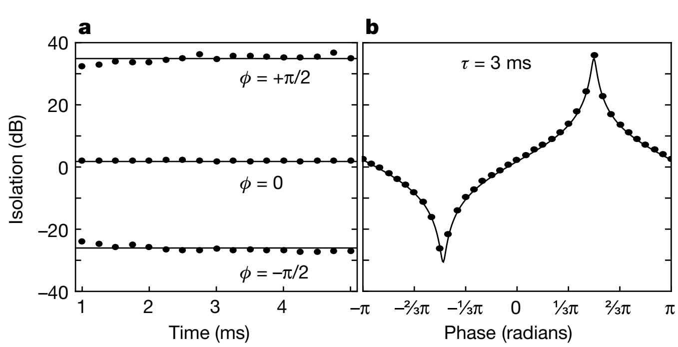

Fig. 3 | Isolation between phononic resonators. The isolation ratio I as a function of the control tones' duration τ (**a**) and phase ϕ (**b**). The values of I are extracted from the data in Fig. 2. The error bars for the statistical uncertainties are smaller than the symbols. The solid lines are the theoretical prediction described in the main text.

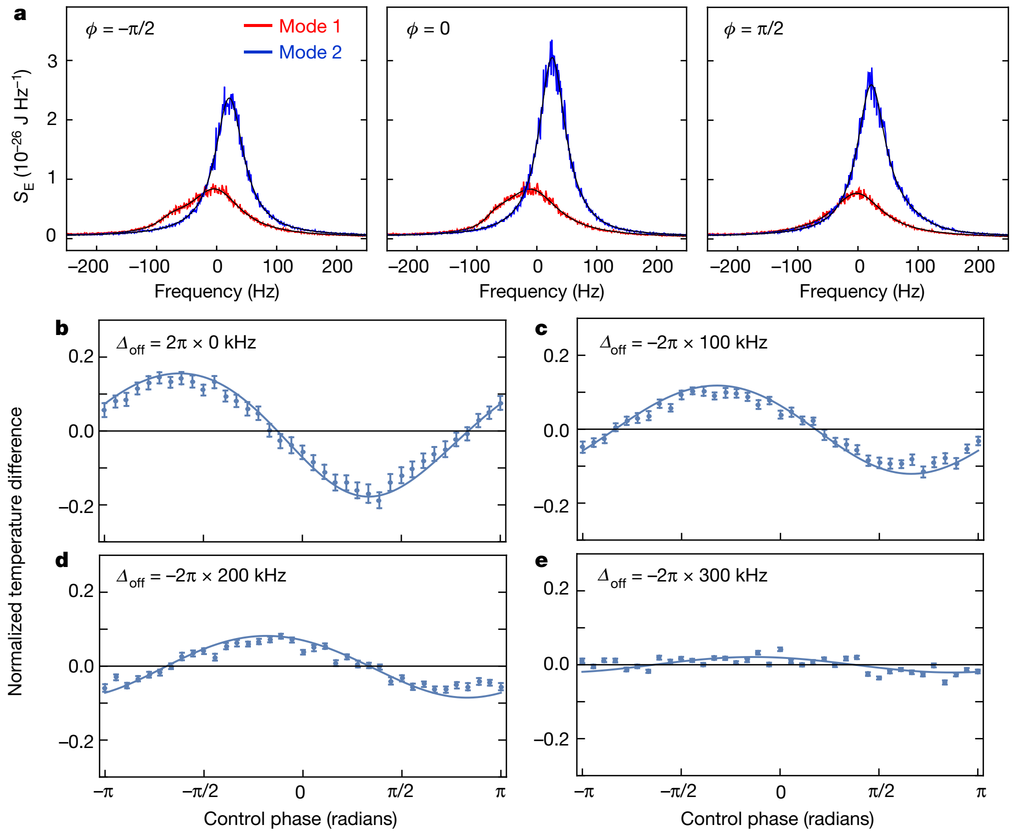

Fig. 4 | Cooling by nonreciprocity. a, The power spectral density of the two modes' thermal motion. For clarity, the data have been offset horizontally so that the two modes (which oscillate at 557 kHz and 705 kHz) can be compared directly. From left to right, the three panels correspond to $\phi = -\pi/2$, 0 and $+\pi/2$. **b–e**, The normalized difference between the two modes' temperatures. The standard error of the mean is indicated by the error bars. In each panel, the control beam detunings are as given in the main text, plus an additional offset Δ_{off}.

this shows that the nonreciprocity demonstrated here represents an additional resource for controlling the thermal fluctuations of phononic resonators.

In conclusion, we have demonstrated a robust, compact, stationary and tunable scheme for inducing nonreciprocity between phononic resonators. We have applied this nonreciprocal control to external signals as well as to the resonators' thermal motion. The nonreciprocity is produced by a cavity optomechanical interaction, but the same scheme may be realized in other multimode oscillator systems with parametric controls, including those in the electrical, mechanical and optical domains[31–33].

Online content

Any methods, additional references, Nature Research reporting summaries, source data, statements of data availability and associated accession codes are available at https://doi.org/10.1038/s41586-019-1061-2.

Received: 10 July 2018; Accepted: 30 January 2019;
Published online 3 April 2019.

1. Jalas, D. et al. What is—and what is not—an optical isolator. *Nat. Photon.* **7**, 579–582 (2013).
2. Fleury, R., Sounas, D., Haberman, M. R. & Alù, A. Nonreciprocal acoustics. *Acoust. Today* **11**, 14–21 (2015).
3. Lewis, M. F. & Patterson, E. Acoustic-surface-wave isolator. *Appl. Phys. Lett.* **20**, 276–278 (1972).
4. Camley, R. E. Nonreciprocal surface waves. *Surf. Sci. Rep.* **7**, 103–187 (1987).
5. Sasaki, R., Nii, Y., Iguchi, Y. & Onose, Y. Nonreciprocal propagation of surface acoustic wave in Ni/$LiNbO_3$. *Phys. Rev. B* **95**, 020407 (2017).
6. Liang, B., Guo, X. S., Tu, J., Zhang, D. & Cheng, J. C. An acoustic rectifier. *Nat. Mater.* **9**, 989–992 (2010).
7. Boechler, N., Theocharis, G. & Daraio, C. Bifurcation-based acoustic switching and rectification. *Nat. Mater.* **10**, 665–668 (2011).
8. Popa, B.-I. & Cummer, S. A. Non-reciprocal and highly nonlinear active acoustic metamaterials. *Nat. Commun.* **5**, 3398 (2014).
9. Fleury, R., Sounas, D. L., Sieck, C. F., Haberman, M. R. & Alù, A. Sound isolation and giant linear nonreciprocity in a compact acoustic circulator. *Science* **343**, 516–519 (2014).
10. Xu, H., Mason, D., Jiang, L. & Harris, J. G. E. Topological energy transfer in an optomechanical system with an exceptional point. *Nature* **537**, 80–83 (2016).
11. Xu, H., Mason, D., Jiang, L. & Harris, J. G. E. Topological dynamics in an optomechanical system with highly non-degenerate modes. Preprint at https://arxiv.org/abs/1703.07374 (2017).
12. Ruesink, F., Miri, M.-A., Alù, A. & Verhagen, E. Nonreciprocity and magnetic-free isolation based on optomechanical interactions. *Nat. Commun.* **7**, 13662 (2016).
13. Huang, P. et al. Nonreciprocal radio frequency transduction in a parametric mechanical artificial lattice. *Phys. Rev. Lett.* **117**, 017701 (2016).
14. Sounas, D. L. & Alù, A. Non-reciprocal photonics based on time modulation. *Nat. Photon.* **11**, 774–783 (2017).
15. Peterson, G. A. et al. Demonstration of efficient nonreciprocity in a microwave optomechanical circuit. *Phys. Rev. X* **7**, 031001 (2017).
16. Bernier, N. R. et al. Nonreciprocal reconfigurable microwave optomechanical circuit. *Nat. Commun.* **8**, 604 (2017).
17. Barzanjeh, S. et al. Mechanical on-chip microwave circulator. *Nat. Commun.* **8**, 953 (2017).
18. Ruesink, F., Mathew, J. P., Miri, M.-A., Alù, A. & Verhagen, E. Optical circulation in a multimode optomechanical resonator. *Nat. Commun.* **9**, 1798 (2018).
19. Aspelmeyer, M., Kippenberg, T. & Marquardt, F. Cavity optomechanics. *Rev. Mod. Phys.* **86**, 1391–1452 (2014).
20. Zwickl, B. M. et al. High quality mechanical and optical properties of commercial silicon nitride membranes. *Appl. Phys. Lett.* **92**, 103125 (2008).
21. Buchmann, L. F. & Stamper-Kurn, D. M. Nondegenerate multimode optomechanics. *Phys. Rev. A* **92**, 013851 (2015).
22. Weaver, M. J. et al. Coherent optomechanical state transfer between disparate mechanical resonators. *Nat. Commun.* **8**, 824 (2017).
23. Metelmann, A. & Clerk, A. A. Nonreciprocal photon transmission and amplification via reservoir engineering. *Phys. Rev. X* **5**, 021025 (2015).
24. Ranzani, L. & Aumentado, J. Graph-based analysis of nonreciprocity in coupled-mode systems. *New J. Phys.* **17**, 023024 (2015).
25. Fang, K. et al. Generalized non-reciprocity in an optomechanical circuit via synthetic magnetism and reservoir engineering. *Nat. Phys.* **13**, 465–471 (2017).
26. Malz, D. et al. Quantum-limited directional amplifiers with optomechanics. *Phys. Rev. Lett.* **120**, 023601 (2018).

27. Barzanjeh, S., Aquilina, M. & Xuereb, A. Manipulating the flow of thermal noise in quantum devices. *Phys. Rev. Lett.* **120**, 060601 (2018).
28. Clerk, A. A., Devoret, M. H., Girvin, S. M., Marquardt, F. & Schoelkopf, R. J. Introduction to quantum noise, measurement, and amplification. *Rev. Mod. Phys*. **82**, 1155–1208 (2010).
29. Yamamoto, K., Otsuka, S., Ando, M., Kawabe, K. & Tsubono, K. Experimental study of thermal noise caused by an inhomogeneously distributed loss. *Phys. Lett. A* **280**, 289–296 (2001).
30. Schwarz, C. et al. Deviation from the normal mode expansion in a coupled graphene-nanomechanical system. *Phys. Rev. Appl*. **6**, 064021 (2016).
31. Unterreithmeier, Q. P., Weig, E. M. & Kotthaus, J. P. Universal transduction scheme for nanomechanical systems based on dielectric forces. *Nature* **458**, 1001–1004 (2009).
32. Teufel, J. D. et al. Circuit cavity electromechanics in the strong-coupling regime. *Nature* **471**, 204–208 (2011).
33. Okamoto, H. et al. Coherent phonon manipulation in coupled mechanical resonators. *Nat. Phys*. **9**, 480–484 (2013).

Acknowledgements This work is supported by the Air Force Office of Scientific Research grant number FA9550-15-1-0270, the Air Force Office of Scientific Research Multidisciplinary University Research Initiative grant number FA9550-15-1-0029, the Office of Naval Research Multidisciplinary University Research Initiative grant number N00014-15-1-2761 and the Simons Foundation (award number 505450).

Reviewer information *Nature* thanks Claudiu Genes, Andre Xuereb and the other anonymous reviewer(s) for their contribution to the peer review of this work.

Author contributions H.X., A.A.C. and J.G.E.H. designed the study. H.X. and L.J. carried out the measurements. H.X. and L.J. analysed the data. All authors contributed to the writing of the manuscript.

Competing interests The authors declare no competing interests.

Additional information
Extended data is available for this paper at https://doi.org/10.1038/s41586-019-1061-2.
Reprints and permissions information is available at http://www.nature.com/reprints.
Correspondence and requests for materials should be addressed to J.G.E.H.
Publisher's note: Springer Nature remains neutral with regard to jurisdictional claims in published maps and institutional affiliations.

METHODS

Theoretical model. We consider two phonon modes coupled to a single optical mode[34] via the usual optomechanical interaction described by the Hamiltonian $H_{\mathrm{OM}}=\sum_{n=1}^{2}\hbar g_n(c_n+c_n^\dagger)a^\dagger a$. Here $\hbar$ is the reduced Planck's constant, g_n is the single-photon coupling strength between the nth phonon mode and the optical mode, a is the optical mode's annihilation operator, and c_n is the annihilation operator for the nth phonon mode[19,34]. The equations of motion for the modes are then:

$$\dot{c}_1=-\left(\frac{\gamma_1}{2}+i\omega_1\right)c_1-ig_1a^\dagger a+\sqrt{\gamma_1}\eta_1 \quad (1)$$

$$\dot{c}_2=-\left(\frac{\gamma_2}{2}+i\omega_2\right)c_2-ig_2a^\dagger a+\sqrt{\gamma_2}\eta_2 \quad (2)$$

$$\dot{a}=-\left(\frac{\kappa}{2}+i\Omega_c\right)a-i(g_1(c_1+c_1^\dagger)+g_2(c_2+c_2^\dagger))a+\sqrt{\kappa_{\mathrm{in}}}a_{\mathrm{in}} \quad (3)$$

where Ω_c is the cavity resonance frequency, and η_i and a_{in} are the drives for, respectively, the phonon modes and the optical mode.

The cavity is driven by two pairs of control lasers to induce nonreciprocity between the phonon modes. The control lasers' detunings (with respect to the cavity resonance) are: $\Delta_1=-\omega_1+\Delta_\ell+\zeta$, $\Delta_2=-\omega_2+\Delta_\ell$, $\Delta_3=-\omega_1+\Delta_{\mathrm{u}}+\zeta$, $\Delta_4=-\omega_2+\Delta_{\mathrm{u}}$. Numerical values for these detunings are given in the main text (note that $\zeta\ll\omega_1,\omega_2,\Delta_\ell$ and Δ_{u}).

Stokes and anti-Stokes scattering of these control lasers can convert a phonon from one mechanical mode to the other. To describe this process quantitatively, we first linearize the optical field by the displacement $a=\alpha+d$, where α is the coherent amplitude of the optical mode and d is the mode's fluctuations. The linearized optomechanical interaction is then $H_{\mathrm{OM,lin}}=\sum_{n=1}^{2}\hbar g_n(c_n+c_n^\dagger)(\alpha^*d+\alpha d^\dagger)$ where $\alpha=\sum_{k=1}^{4}\alpha_k\mathrm{e}^{-i\Delta_k t}$ and α_k is the coherent amplitude contributed by the kth control laser.

The parameters of the experiment are such that the mechanical resonance frequencies and the separation between the motional sidebands are always much greater than the mechanical linewidths. As a result, the cavity field can be adiabatically eliminated to obtain the effective Hamiltonian for the mechanical modes:

$$H=\sum_{n=1}^{2}\hbar(\omega_n-i\gamma_n/2+\sigma_{n,n})c_n^\dagger c_n+\sigma_{1,2}\mathrm{e}^{i\Delta t}c_1^\dagger c_2+\sigma_{2,1}\mathrm{e}^{-i\Delta t}c_2^\dagger c_1 \quad (4)$$

where

$$\sigma_{n,n}=\sum_{k=1}^{4}i\hbar g_n^2|\alpha_k|^2(\chi(\omega_n-\Delta_k)-\chi(\omega_n+\Delta_k)) \quad (5)$$

$$\sigma_{1,2}=\sum_{k=1}^{2}i\hbar g_1g_2\alpha_{2k-1}^*\alpha_{2k}\mathrm{e}^{i(k-1)\phi}(\chi(\omega_1-\Delta_{2k})-\chi(\omega_1+\Delta_{2k-1})) \quad (6)$$

$$\sigma_{2,1}=\sum_{k=1}^{2}i\hbar g_1g_2\alpha_{2k-1}\alpha_{2k}^*\mathrm{e}^{-i(k-1)\phi}(\chi(\omega_2-\Delta_{2k-1})-\chi(\omega_2+\Delta_{2k})) \quad (7)$$

and $\chi(\omega)=(\kappa/2-i\omega)^{-1}$. As described in the main text, ϕ is the relative phase between the two beat notes whose frequencies are nearly equal to $\delta\omega$.

Temperature measurement. As with any driven optomechanical system, our system is not strictly in thermal equilibrium, and so one needs to specify exactly what is meant by the effective temperature of each mechanical mode. We recap here the standard approach to this problem (see, for example, ref. [28] for a pedagogical review).

For a stationary, non-equilibrium system, one can define at each frequency an effective temperature by considering the ratio of fluctuations to dissipation at that frequency. Letting $-\chi_{xx}[\omega]$ denote the full mechanical force susceptibility of the mode of interest (that is, $\chi_{xx}[\omega]$ is the retarded position–position Green's function of the mode), we have:

$$\coth\left[\frac{\hbar\omega}{2k_{\mathrm{B}}T_{\mathrm{eff}}[\omega]}\right]\equiv\frac{\bar{S}_{xx}[\omega]}{-\hbar\,\mathrm{Im}\,\chi_{xx}[\omega]} \quad (8)$$

For a system in thermal equilibrium, $T_{\mathrm{eff}}[\omega]$ would be equal to the physical temperature T at all frequencies. In the classical regime of interest here, where effective temperatures are much larger than the frequencies of interest, this relation becomes:

$$k_{\mathrm{B}}T_{\mathrm{eff}}[\omega]\equiv\frac{\bar{S}_{xx}[\omega]}{-2\,\mathrm{Im}\,\chi_{xx}[\omega]/\omega} \quad (9)$$

It follows that the position fluctuations $\langle x^2\rangle$ are essentially a weighted integral of $T_{\mathrm{eff}}[\omega]$:

$$\langle x^2\rangle=\int\frac{\mathrm{d}\omega}{2\pi}\bar{S}_{xx}[\omega]=\int\frac{\mathrm{d}\omega}{2\pi}\left(\frac{-2\,\mathrm{Im}\,\chi_{xx}[\omega]}{\omega}\right)k_{\mathrm{B}}T_{\mathrm{eff}}[\omega] \quad (10)$$

We can thus use $\langle x^2\rangle$ to define a single effective temperature $\overline{T}$ to describe the mode, which will be a weighted average of the frequency-dependent effective temperature $T_{\mathrm{eff}}[\omega]$:

$$k_{\mathrm{B}}\overline{T}=k_{\mathrm{eff}}\langle x^2\rangle \quad (11)$$

where the effective spring constant is defined as

$$\frac{1}{k_{\mathrm{eff}}}=\int\frac{\mathrm{d}\omega}{2\pi}\left(\frac{-2\,\mathrm{Im}\,\chi_{xx}[\omega]}{\omega}\right) \quad (12)$$

Using the Kramers–Kronig relation, we obtain

$$\frac{1}{k_{\mathrm{eff}}}=-\chi_{xx}[\omega=0] \quad (13)$$

We use the above definition of $\overline{T}$ to define the effective temperature for each mechanical mode in the main text.

We make some important remarks on this procedure. First, if our oscillator was truly in thermal equilibrium at a temperature T, then (via the fluctuation dissipation theorem) $\overline{T}=T$, irrespective of the particular shape of $\chi_{xx}[\omega]$. Thus our definition does not require the mechanical mode to have a simple Lorentzian resonance. Second, for a standard damped mechanical harmonic oscillator of mass m, spring constant k_0 and damping rate γ, the susceptibility takes the usual form:

$$\chi_{xx}[\omega]=\frac{1}{m}\times\frac{1}{\omega^2-\Omega^2+i\omega\gamma} \quad (14)$$

with $\Omega=(k/m)^{1/2}$. In this case, $k_{\mathrm{eff}}=k_0$ (that is, it is just the spring constant of the mode), recovering the usual equipartition theorem.

For application to our system, we note that the modification of the mechanical susceptibility of each mode due to optomechanical interactions implies that k_{eff} could in principle deviate from k_0. By explicitly calculating $\chi_{xx}[\omega]$ from H (which is defined in the main text) and using equation (13), we find that k_0 and k_{eff} differ by about 10^{-4}, which is insignificant. We thus use equation (11) to define the effective temperature $\overline{T}$ of each mode from the measured position fluctuation spectral density, using the bare spring constant, that is, with $k_{\mathrm{eff}}\rightarrow k_0$.

Data availability

The datasets generated during and/or analysed during the current study are available from the corresponding author on reasonable request.

34. Shkarin, A. B. et al. Optically mediated hybridization between two mechanical modes. *Phys. Rev. Lett.* **112**, 013602 (2014).

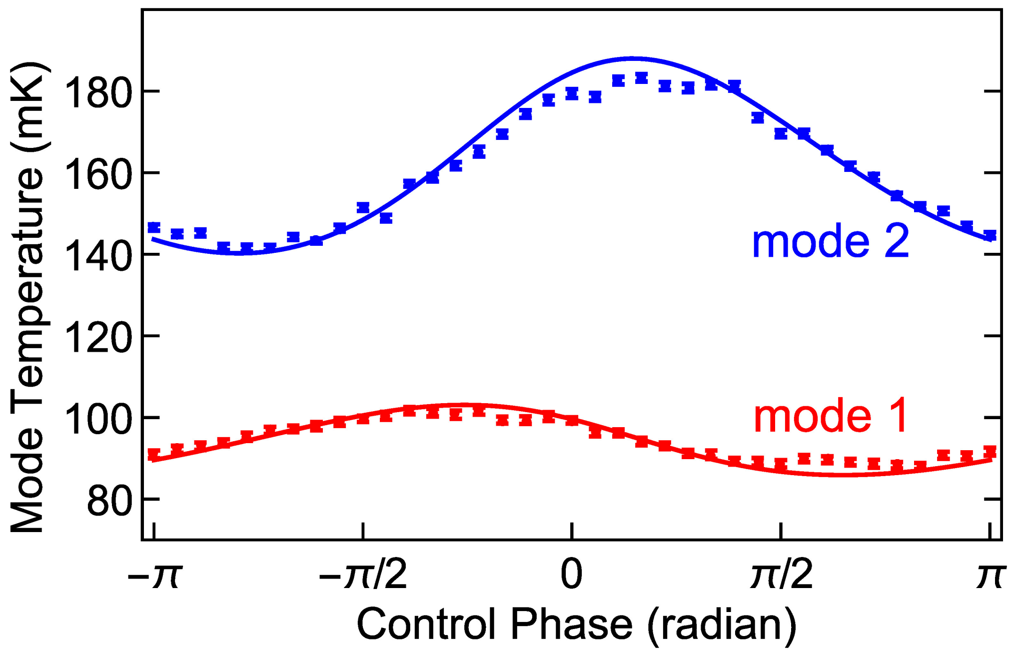

Extended Data Fig. 1 | Temperature of each phononic mode as a function of the control tone phase. This data was used to calculate the normalized temperature ratio shown in Fig. 4b. The error bars show the standard error of the mean.